Electronic energy bands of lead: Angle-resolved photoemission and band-structure calculations

K. Horn
Fritz-Haber-Institut der Max-Planck-Gesellschaft, D-1000 Berlin 33, West Germany

B. Reihl,* A. Zartner, and D. E. Eastman
IBM Thomas J. Watson Research Center, Yorktown Heights, New York 10598

K. Hermann and J. Noffke
Institut für Theoretische Physik der Technischen Universität Clausthal and Sonderforschungbereich 126 Clausthal/Göttingen, D-3392 Clausthal Zellerfeld, West Germany
(Received 6 January 1984; revised manuscript received 23 April 1984)

Angle-resolved photoemission with synchrotron radiation was applied to Pb(111) in order to determine the electronic band structure of Pb. The ΓL direction was mapped out by recording normal-emission photoelectron spectra. Band energies at several symmetry points in the Brillouin zone were obtained by evaluation of off-normal spectra. An adjusted free-electron parabola describes the empty bands well when compared with the critical points resulting from our band-structure calculation using the self-consistent linear rigorous cellular method. The occupied bands close to the Fermi energy agree well with theory, particularly with respect to the magnitude of the spin-orbit splitting, whereas there are discrepancies for the lowest occupied valence band. Inelastic scattering of photoelectrons gives rise to additional peaks in the spectra which cannot be attributed to direct transitions. No surface state was observed in the *s-p* band gap.

I. INTRODUCTION

The knowledge of the electronic band structure of a solid is fundamental to our understanding of its physical properties. Historically, the experimental determination of metal band structures has been restricted to an investigation of the Fermi surface, e.g., by de Haas—van Alphen measurements. The determination of energy differences between certain points in the Brillouin zone through reflectivity measurements has also contributed to band-structure investigations. However, a number of recent studies have shown[1] that, by means of angle-resolved photoemission, particularly when used in conjunction with polarized and tunable synchrotron radiation, the full band structure of solids can be determined with high accuracy. Such experimental band structures in many cases show good agreement with state-of-the-art band-structure calculations.

A great deal of attention in these studies has been paid to the noble metals[2–4] and the group-VIII*b* metals,[5,6] whereas only a few experiments have dealt with those where the valence levels have *s-p* character.[7–10] This has led us to study the band structure of Pb, which has so far only been studied by x-ray photoemission (XPS) and angle-integrated ultraviolet (uv) photoemission.[11,12] The band structure of lead is also interesting because spin-orbit-interaction effects are manifest in a clear manner.

II. EXPERIMENTAL METHODS

The photoemission experiments were performed with a two-dimensional display-type electron spectrometer described previously.[13] Synchrotron radiation from the 240-MeV storage ring TANTALUS at the Synchrotron Radiation Center of the University of Wisconsin—Madison, dispersed by a 3-m toroidal-grating monochromator was used for photoexcitation; the combined resolution of monochromator and analyzer was about 200 meV in the angle-integrating mode.[13] The Pb(111) crystal was spark-cut from a single-crystal boule and mechanically polished. It was etched in a 1:1 acetic acid:hydrogen peroxide solution and rinsed in methanol immediately prior to loading in the vacuum chamber by means of a fast-entry vacuum airlock. *In situ* cleaning was performed by argon-ion bombardment and annealing to 175 °C. No traces of carbon, oxygen, or other impurities were detectable in the Auger-electron spectra, and the crystal produced a clear (1×1) low-energy electron diffraction (LEED) pattern. All experiments were carried out at room temperature.

III. RESULTS AND DISCUSSION

An angle-integrated photoelectron spectrum of a clean Pb(111) surface, recorded at a photon energy of 60 eV, is shown in Fig. 1. In the valence region of the spectrum, broad peaks centered at 2.5 and 8.5 eV below the Fermi energy E_F are observed, well separated by a valley at about 5 eV; strong emission from the Pb 5*d* levels occurs at 17.9 and 20.6 eV below E_F. In addition, broad peaks which do not shift with $\hbar\omega$ are observed at 2.3, 5.6, and 10.1 eV kinetic energy (not shown in Fig. 1). The electronic-level occupation in lead is $5d^{10}6s^26p^2$; the valence bands therefore consist of *s-p*-like bands. From the low-energy cutoff in the spectra the work function of clean Pb(111) was determined to be 3.8 eV.

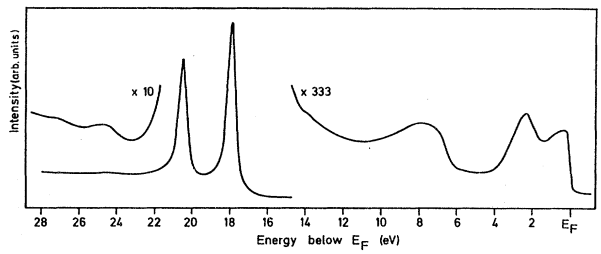

FIG. 1. Angle-integrated photoelectron spectra of clean Pb(111) recorded at a photon energy of 60 eV, showing the valence region and the $5d$ core levels.

A. Interpretation of normal-emission spectra

A common method for the determination of the valence-band structure by photoemission is to record spectra in normal emission for a wide range of photon energies, from a crystal with a high-symmetry orientation. The electron-momentum component normal to the surface, $\vec{k}_\perp$ is not conserved because of the potential barrier at the surface. It is then necessary to determine the final-state dispersion in order to identify the direct transitions giving rise to peaks at particular photon energies. The assumption that the unoccupied bands can be approximated by a free-electron-like parabola has been successfully used in many cases.[1] The bottom energy of this parabola, sometimes called the "inner potential," is used as an adjustable parameter which is fitted to give the best agreement with the observed dispersion effects. By using such a final band and constructing the direct transitions appropriate for the particular photon energies, the occupied bands can be determined. One must be aware of the approximations involved at this stage, particularly near zone boundaries where the deviations from free-electron-like behavior are known to be large.

Ideally, one would like to rely on final bands which are calculated in a scheme where the final state is properly described by a time-reversed LEED state. In favorable cases, the shape of the band structure facilitates the fitting of the unoccupied bands. Consider the spectra recorded from clean Pb(111) at normal emission and varying photon energy shown in Fig. 2. In the spectrum at a photon energy of 22 eV, a peak appears close to the Fermi level, which shifts to higher binding energies with increasing photon energies. This indicates that a band crosses the Fermi level, which proves to be of great value for the band-structure evaluation, since the $\vec{k}$ value of this point which lies on the Fermi surface has been accurately determined by Anderson and Gould[14] using de Hass—van Alphen data. Thus we know the energy of the initial as well as final band at this particular point in $\vec{k}$ space, and this gives an unambiguous value for the determination of our free-electron parabola. Since we know the approximate bandwidth from spectra recorded at many different angles and photon energies, the size of the gap between the upper band close to E_F and the lower, s-like band is determined to be approximately 3.2 eV at L. We therefore have a good basis for the determination of the occupied p-like (upper) band. This information is the basis for the experimental band structure shown in Fig. 3, where the free-electron parabola is shown as a dotted-dashed line. The peak positions in the other spectra of Fig. 2, shown by arrows, as well as additional spectra, are then evaluated using the free-electron final band mentioned above. They are plotted as a function of $\vec{k}$ in Fig. 3. The band close to E_F can be determined quite accurately in the range 0 to 4 eV below E_F, and is compared with the calculated band structure in Sec. IV. The evaluation of the lower (7 to 10.5 eV below E_F) band is impeded by strong broadening of the peaks. This $\vec{k}$ broadening, marked by an asterisk in Fig. 2, is partly due to the short mean free path of photoelectrons which destroys the $E(\vec{k})$ information in many high-Z materials.[15] It masks peak shifts due to direct transitions, an effect which is also evident in the region near the Fermi level, for example, in a broad peak at about 2 eV which does not shift with photon energy. All peaks are rather broad (1 to 1.5 eV), even at E_F, where hole lifetimes do not have a strong broadening influence. These broadening effects are most likely due to photoelectrons which have undergone inelastic forward scattering from bulk and/or surface phonons following the photoexcitation process.

In this study spectra were only recorded at room temperature. Petroff and co-workers[16] have recently recorded

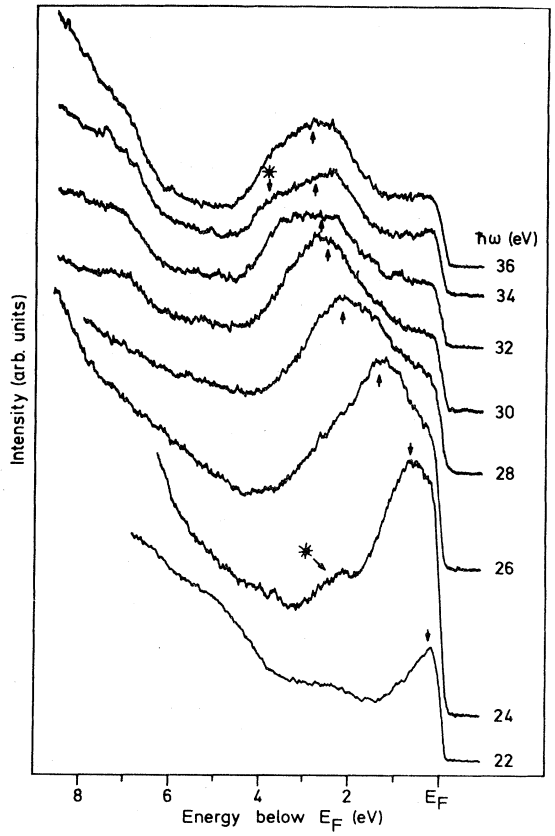

FIG. 2. Angle-resolved photoelectron spectra from Pb(111), recorded in normal emission at photon energies as indicated.

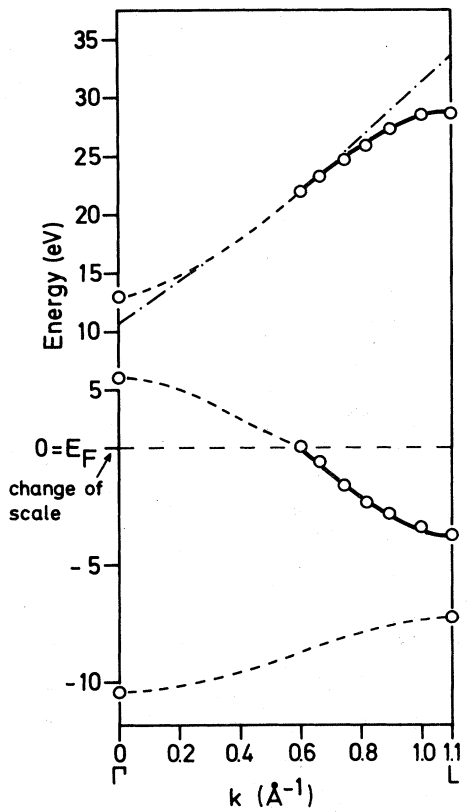

FIG. 3. Experimental band structure of Pb(111) along the Γ—L line, derived from the spectra of Fig. 2. The position of the band crossing E_F has been taken from de Haas—van Alphen data in Ref. 14.

angle-resolved photoelectron spectra from Pb(110) over a wide range of temperatures. They observed that, at low temperatures (approximately 10 K) where scattering by phonons is greatly reduced, all peaks in the spectrum are much narrower and can be attributed to direct transitions. However, broadening effects completely dominate the spectrum at 300 K such that a band-structure determination was possible *on Pb(110)* only at low temperature. This indicates that it is the *surface* Debye temperature which is important for the assessment of the amount of inelastic scattering, since our spectra from Pb(111) show that a band-structure determination from this surface, while being affected by the scattering processes, is nevertheless possible. On the more open (110) face the peaks due to direct transitions seem to be totally masked by the scattered electrons in room-temperature spectra. This is in line with LEED determinations of the surface Debye temperature of lead surfaces, which yield a value of 49 K for the close-packed (111) surface; on the (110) surface this value is 37 K, i.e., 40% of the bulk Debye temperature.[17] It is therefore plausible that an interpretation of the room-temperature spectra is more likely to be successful on the (111) than on the (110) face.

While the shape of the occupied upper band can be determined despite the effect of $\vec{k}$ broadening on the spectra, the peaks due to the lower band are so strongly affected that only its energies at the zone boundaries can be determined with accuracy from the total-energy range at which this peak appears at different photon energies and emission angles; the shape of the band away from Γ and L can only be interpolated. This is indicated in Fig. 3 by the dashed-dotted line. Above 32 eV, a band gap occurs in the calculated empty bands. Here transitions from the occupied bands to evanescent states located in the selvedge region occur, such that no dispersion effects are expected,[18] and none are in fact observed in our spectra. In addition, inelastic scattering effects become more pronounced at higher electron energies,[15,19] such that little information about the band dispersion can be extracted from the spectra recorded at photon energies higher than about 50 eV. The peaks in the secondary region of the spectrum, which do not shift with photon energy, provide some information on the unoccupied bands, since these peaks correspond to photoelectrons which are inelastically scattered upon transport to the surface, and are then emitted at energies of points of high density of states in the unoccupied bands; such peaks have been observed with Cu and Ag.[20] Their positions are therefore marked by circles in the unoccupied region of the band structure at Γ.

An interesting aspect is the absence of a surface-state peak in the spectra in the region of the s-p gap in normal emission. As can be seen from the spectra of Fig. 2, no detectable extra emission occurs in this region, at least in the photon-energy range used in this study ($\hbar\omega = 18$ to 55 eV). Occupied surface states in the s-p gap have been observed on the (111) faces of many metals; for example, on Cu,[21] Ni,[22] and Zn.[10] Since there are presently no calculations of the surface electronic structure of Pb(111) available, this conspicuous absence remains unexplained for the time being.

B. Determination of critical-point energies by off-normal spectra

Only s and p states contribute to the occupied bands in lead. The band structure is therefore relatively simple, being dominated by the parabolic shape (strongly modified near zone boundaries) and spin-orbit interaction. In order to decide whether a band-structure calculation correctly describes the bands in lead, it is sufficient to determine the band energies at a few critical points. By evaluating the data in Fig. 3, we have already determined the band energies at Γ and L for the occupied as well as unoccupied bands for energies up to 35 eV. Further information about the band structure may be obtained by recording spectra in normal emission from surfaces cut along other crystallographic directions. A knowledge of the bands at the W point is particularly advantageous since three occupied bands occur there, two of which are separated by spin-orbit interaction, the magnitude of which can be directly evaluated.

A less time-consuming method for a determination of band energies at other points of high symmetry by photoemission from a (111) face uses spectra recorded in directions away from the surface normal. Consider a cut through a three-dimensional Brillouin zone in a repeated-zone scheme, which contains the ΓL axis, i.e, the [111] direction, as well as the ΓKX axis. This is shown in Fig.

4. In the free-electron band model, the final-state wave-vector component normal to the surface $\vec{k}_\perp$ is correlated to the kinetic energy of the photoelectron and its wave-vector component parallel to the surface by

$$|\vec{k}_\perp| = \hbar^{-1}[2m(E-V_0)-\hbar^2|\vec{k}_\parallel|^2]^{1/2},$$

where E is the electron kinetic energy and V_0 is the inner potential. This formula is based on the assumption of direct transitions without surface umklapp processes.[1] The final bands at a particular energy therefore describe circles shown by the thin lines in Fig. 4. Wherever these circles cross the lines, i.e., the Brillouin-zone boundaries, deviations of the real bands from these circles are bound to occur, however [see Fig. 7 in Ref. 2(b)]. The thin parabolas indicate the relation given by the above equation for various polar angles of photoelectron emission. Thus, from the plot in Fig. 4 one would expect to observe photoemission from the U point at a kinetic energy close to 32 eV and a polar angle of about 15°.

By using a conventional electron-energy analyzer which is limited to a particular acceptance angle of typically 2°—4°, many spectra at different polar angles and photon energies have to be recorded in order to search for emission at the critical point, at which the band energies exhibit extremal behavior. The ellipsoidal-mirror display analyzer used in this study offers a more elegant way in which to determine the band energies around such points.

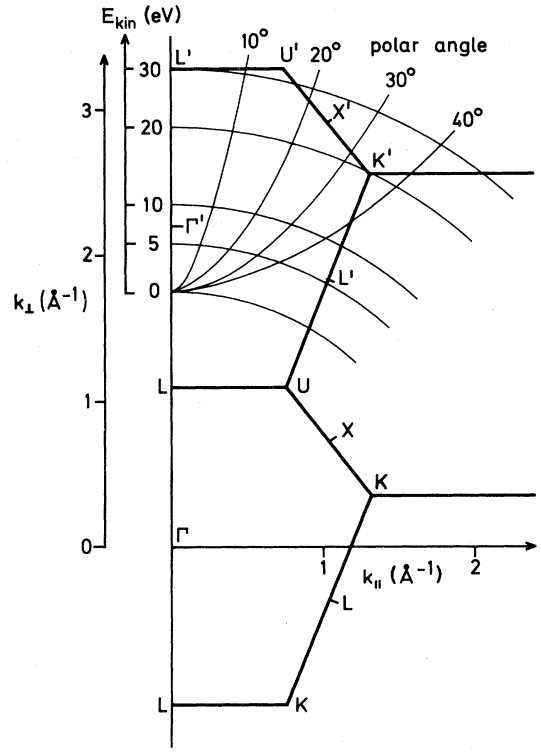

FIG. 4. Cut through an extended Brillouin-zone scheme of a fcc metal in the ΓLUX plane; numbers on the parabola indicate the polar angles, and circles show kinetic energies at which emission from specific points in the Brillouin zone are expected to occur on the basis of the free-electron final state model.

Here, a photoemission picture is recorded, similar to the display in a LEED system, such that different areas in the pattern correspond to particular polar and azimuthal angles of emission at one specific electron kinetic energy. Stated in the free-electron final-band model we observe electron-emission intensity on one of the circles centered around Γ in Fig. 4 or, since we have a two-dimensional display, on a sphere with the radius of curvature of these

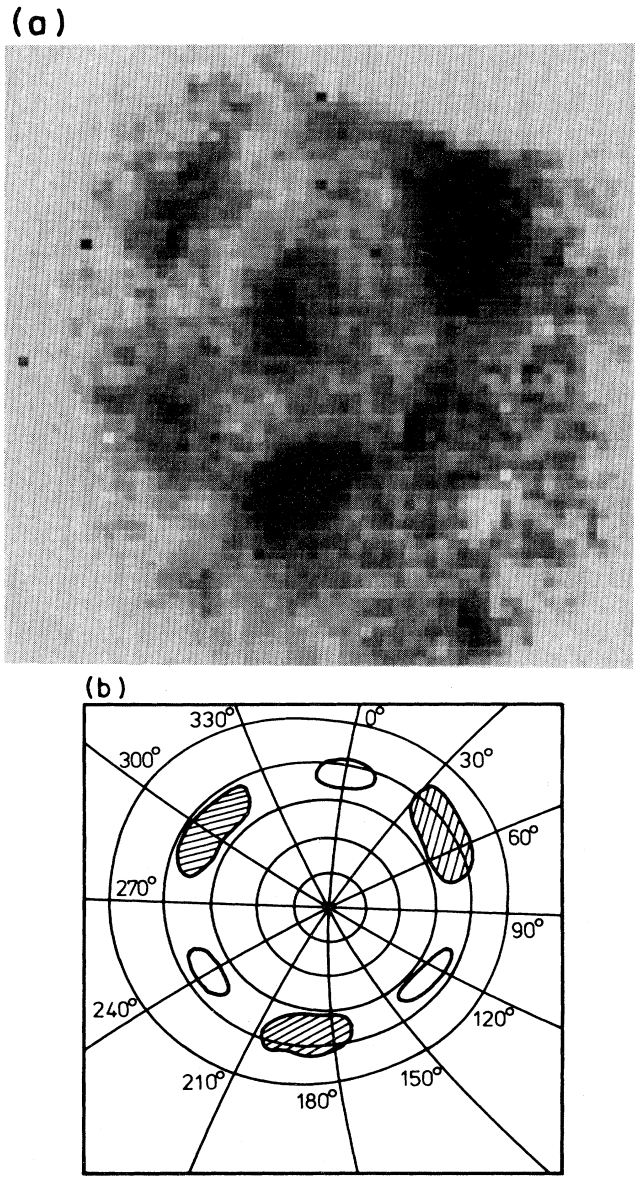

FIG. 5. (a) Photoemission-intensity pattern recorded with the aid of the two-dimensional display electron analyzer at a photon energy of 33 eV and an electron kinetic energy of 26 eV. Dark spots correspond to strong emission. The central spot is the normal-emission direction, while the three dark spots on the outer circle correspond to emission from bands on the $L-K$ line. (b) Sketch of the photoemission-intensity distribution. Polar angles are indicated by distorted circles (for every 5° of emission from normal, which corresponds to the center of the "spider net"). The distortion arises from the geometric arrangement of the channel plates with respect to the axis of the ellipsoidal energy analyzer.

circles. The intensity distribution in such a model is determined by the relative intensity of a peak at a particular energy in different polar and azimuthal directions, i.e., by the symmetry of particular direct transitions and hence by the symmetry of the surface or bulk lattice along the direction being studied. This is demonstrated by the photograph shown in Fig. 5(a), which was recorded with the aid of a digital video processing unit, at a photon energy of 33 eV and an electron binding energy of 3.0 eV below E_F. The dark areas in the photograph correspond to high photoemission intensity. The normal-emission direction is indicated in the contour drawing of the photograph in Fig. 5(b) as the center of the "spider net," and corresponds to the dark spot in the center of the photograph. The polar and azimuthal angles are also indicated in Fig. 5(b); the lines of equal polar angle are distorted circles because of the arrangement of the channel plates and screen with respect to the ellipsoidal-mirror axis. At this particular photon and electron energy, we are probing transitions in a cut slightly below the $L'W'K'$ plane as evident from the diagram in Fig. 4. The pattern therefore possesses a threefold symmetry with respect to the angles at which strong [shown hatched in Fig. 5(b)] and weak emission occurs, which one does expect from photoemission of a (111) face of a fcc metal. The intense spots are due to emission from points of high density of states along the line L'—K', and the weaker spots are related to emission from points along U'—X', each of which have threefold symmetry. The spot intensities need not be similar because of instrumental effects (channel-plate sensitivity)

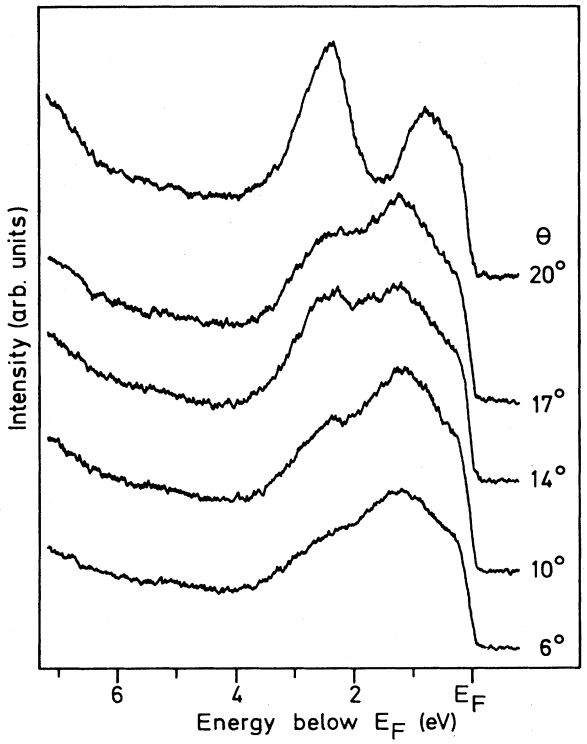

FIG. 6. Series of spectra recorded at different polar angles in the LWK azimuth. Note the increase in emission at a polar angle of 20°.

TABLE I. Comparison of experimental energies of occupied bands at points of high symmetry in the Brillouin zone with the calculated values.

Band	Energy below E_F (eV) Expt.	Calc.
Γ^{6+} (lowest band)	10.5	11.7
L^{6+} (lowest band)	7.0	8.2
L^{6-} (upper band)	3.7	4.3
K^5 (lowest band)	7.0	7.0
K^5 (second band)	2.4	2.6
K^5 (highest band)	1.0	1.1
W^6 (lowest band)	7.0	6.8
W^7 (second band)	2.4	2.2
W^6 (highest band)	0.8	0.7

and matrix-element changes. In the $L'W'K'$ plane, many points of high symmetry contribute to the spectra, such that the photoemission pattern in this plane around the L point resembles a quasihexagonal ring.

The final bands are expected to deviate from parabolic behavior, particularly close to the zone boundaries. Therefore it is necessary to record a series of spectra in the region where band energies are expected to exhibit maxima in order to find the band extrema. A number of such spectra, recorded along the LWK azimuth, i.e., the [112] direction, are shown Fig. 6. Note the increase in intensity in the spectrum at 20° polar angle which is indicative of emission from a band extremum. The resulting band energies at high-symmetry points determined from such a search are indicated in Table I. The third band which drops below the Fermi energy at the K and W points has an energy of 0.8 eV at W and 1.0 eV at K. The magnitude of the spin-orbit splitting which is reflected in the energy separation between the upper W_7 and W_6 points therefore amounts to 1.6 eV, in good agreement with the value of 1.68 eV derived by de Haas—van Alphen measurements.[14] Band energies at specific points of high symmetry in the Brillouin zone are given in Table I.

IV. COMPARISON WITH BAND-STRUCTURE CALCULATIONS

A. Details of the band-structure calculations

Band-structure calculations for Pb, based on the relativistic augmented-plane-wave[23] (RAPW) and other calculational schemes[14,24,25] were published quite early and showed good agreement with available Fermi-surface data[14] and, to some extent, also with XPS valence-band spectra.[11,25] However , these calculations were restricted to the occupied bands and to the region about 5 eV above E_F, such that our experimental determination of the final band could not be tested against these data. We have therefore carried out band-structure calculations of bulk lead over a wide range of energies using the self-consistent

linear rigorous cellular[26] (LRC) method. This method has been shown to yield good quantitative agreement with other band-structure calculation schemes and with photoemission experiments for various metals.[27] The formalism of the LRC method is documented elsewhere.[26,27] Therefore we restrict ourselves to a brief discussion of the input data used in the present calculation. The lattice constant of face-centered-cubic Pb was equal to the experimental value of $a_0=4.95$ Å. For the first iteration the one-electron potential containing non-muffin-tin corrections[26] is constructed from relativistic self-consistent charge densities of the Pb atom using the Hedin-Lundqvist approximation for exchange and correlation.[28] Relativistic effects and spin-orbit coupling are included in the band calculation beyond a perturbational treatment. Self-consistency of the band states is achieved in at most four iterations using a charge-density criterion.

In a first calculation we determine the self-consistent band states of the Pb $6s$ and $6p$ valence electrons where the wave functions of the Pb $1s$ to Pb $5d$ electrons are kept frozen. As a result, Fig. 7 shows the valence-band structure starting from the lowest $6s$-type band up to 32.5 eV above the Fermi level. Here the dotted curves along ΓX denote Δ_7-type bands, while the solid curves refer to the Δ_6 bands. Along ΓL the dotted bands are Λ_{4+5}, whereas the solid bands are of Λ_6 symmetry. This band structure agrees quite well with recent Korringa-Kohn-Rostoker (Ref. 29) and APW (Ref. 30) calculations in the region of the occupied band states. The gap between the occupied $6s$ and $6p$ bands at L is 3.8 eV compared to 3.3 eV from Ref. 26 and 3.5 eV from the experimental data of Fig. 3.

In a second step, we allow for relaxation of the Pb $5d$ electrons and recalculate the band structure self-consistently including the $5d$ bands. The effect of relaxation is, however, quite small, as can be seen from Table II, which compares the band energies at a few high-symmetry points computed with and without the frozen

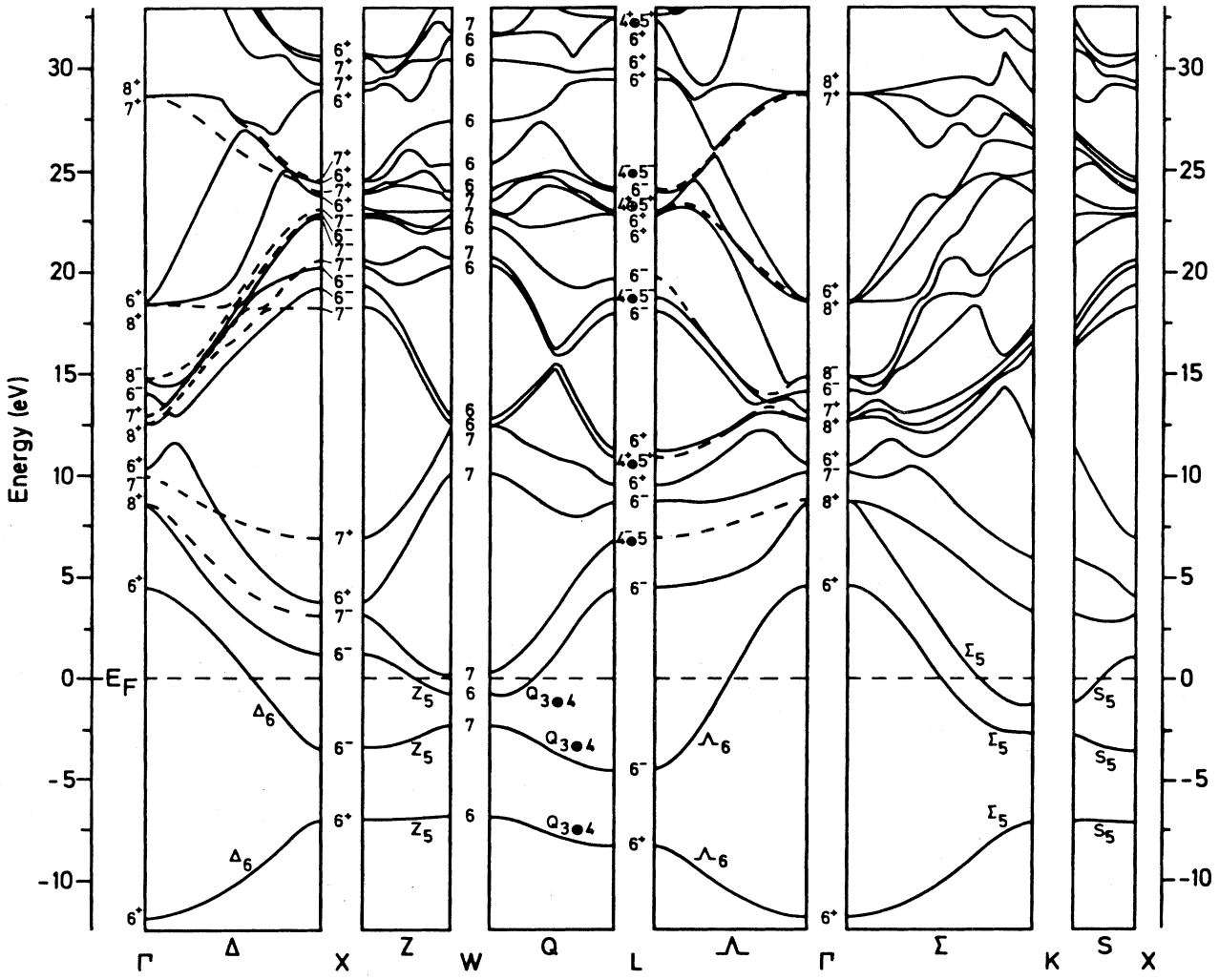

FIG. 7. Self-consistent relativistic band structure for Pb along characteristic high-symmetry directions of the Brillouin zone. The dotted curves along ΓX (ΓL) refer to Δ_7 (Λ_{4+5}) band states while the solid curves belong to Δ_6 (Λ_6) symmetry states. The energies are given with respect to the Fermi level E_F.

TABLE II. Comparison of Pb band energies for high-symmetry prints computed (a) with frozen $5d$-electron wave functions and (b) including the $5d$-band states explicitly. The energies are given in eV.

Γ		X		W		L		K	
(a)	(b)	(a)	(b)	(a)	(b)	(a)	(b)	(a)	(b)
−11.76	−11.66	−6.93	−6.78	−6.76	−6.63	−8.24	−8.10	−6.95	−6.82
		−3.34	−3.37	−2.25	−2.28	−4.43	−4.41	−2.67	−2.67
				−0.68	−0.65			−1.05	−1.09

$5d$ wave functions. The difference turns out to be less than 0.15 eV.

B. Comparison between theoretical and experimental data

In our comparison with the calculated bands using the scheme outlined above, we first consider the occupied bands. The theoretical and experimental band energies at several critical points throughout the Brillouin zone are compared in Table I. Agreement is good for the band close to E_F. There is some discrepancy with respect to the upper and lower boundary of the lower band. The calculation places the bottom of this band at about 11.8 eV, while the experimental value is (10.5±0.5) eV. The same discrepancy occurs at the top of this band. It was suspected that the proximity of the $5d$ levels might push the lower band closer to E_F. An inclusion of the $5d$ states into the calculation did not, however, bring about any improvement in the agreement of theory and experiment with respect to this point as outlined above. It is likely that the disagreement is caused by the large uncertainty in the experimental determination of this particular band (see Sec. III).

Some caution is needed when comparing theoretical and experimental final bands. If we omit the final bands inaccessible in normal emission because of symmetry-selection rules (these are shown as dashed lines in Fig. 7), there are still several bands which must be considered. In the theoretical band structure, ground-state unoccupied bands are calculated, while in the experiment the excited state with a hole in the valence band is probed. The response of the solid to the creation of a hole is bound to affect the bands in the hole state. Thus a comparison between theory and experiment is only meaningful under the assumption that the ground-state bands and the excited-state bands do not differ too much. In practice, the comparison between experimental band energies and the ground-state band calculations seems to work well in many cases. Hole lifetimes also affect the experimental band structure; this is sometimes accounted for by using a complex band structure, where photoemission is allowed even in a gap region between the unoccupied bands. Here photoelectrons couple to evanescent states located in the selvedge region. Furthermore, the calculation is made for bulk lead, neglecting surface effects which are bound to play an important role in our investigations. The small escape depth of the photoelectrons in the range between 20 and 35 eV kinetic energy will lead to a broadening and therefore an averaging of $\vec{k}$.

Keeping these restrictions in mind we compare in Fig. 8 the theoretical unoccupied bands and our experimental final band. It is evident that our modified free-electron parabola (solid curve) is broken into several bands in the calculated band structure (shown as dashed-dotted lines), but sections of the calculated bands are very similar in shape and location to the free-electron parabola. Those parts which are similar to the parabola represent valid final states for electron emission. The parts of the theoretical bands beyond the energy maximum, where the energy

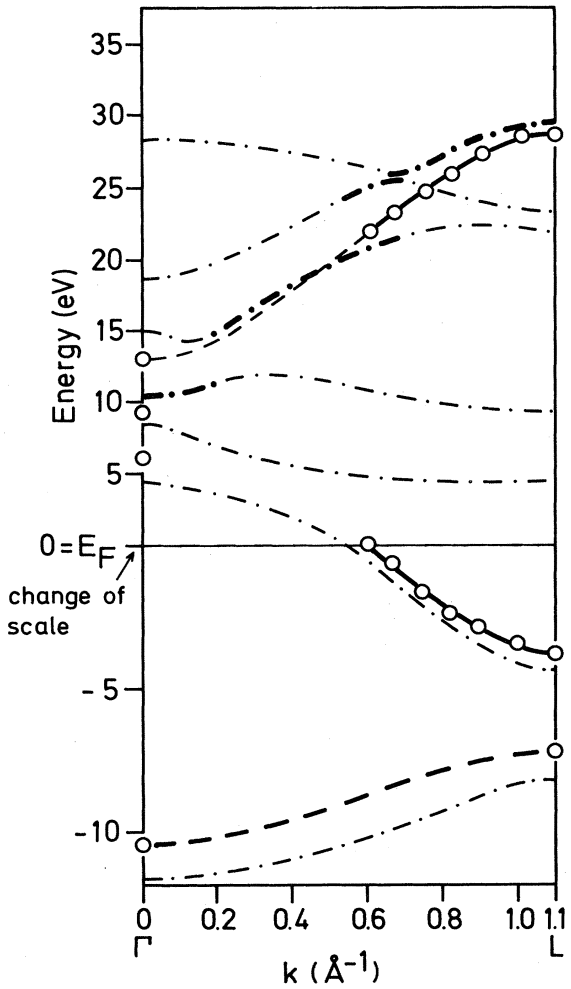

FIG. 8. Comparison of experimental bands (from Fig. 3) and calculated bands along ΓL. Circles denote the experimentally derived values. Dotted-dashed lines indicate calculated bands (enhanced in the regions where they are close to the free-electron-like parabola).

decreases with $\vec{k}$, for example, close to L at 22 and 25 eV above E_F, corresponds to electrons propagating into the crystal; this can be seen from an evaluation of the electron group velocities.[31] The lower and rather flat bands which lie in the region 5 to 10 eV above E_F need not be considered here since they correspond to inaccessible transitions due to a low photoionization cross section at photon energies below 18 eV. From Fig. 8 it is evident that fair agreement exists between theoretical unoccupied and experimental final bands as far as the band maxima and minima at 6, 11, and 16 eV are concerned, which correspond to the features which appear in the secondary part of the spectrum. The band maximum at 29 eV is also present in both theory and experiment. For energies between 20 and 30 eV, however, the free-electron parabola is split into several bands in the calculated band structure.

The question why the free-electron parabola is such a good basis for bulk band determinations by angle-resolved photoemission was recently treated by Hora and Scheffler.[32] They calculated the photoelectron spectrum from a Pd(111) crystal using the one-step model, which is by far the most sophisticated approach presently used. In order to assess the value of the various approximations currently in use, they also performed calculations using a single-particle potential of the ground state. Their results show that the angle-resolved photoelectron spectrum can be understood in terms of direct transitions if the inelastic electron-electron interaction in the final state is taken into account. It is shown that the final bands calculated by using the ground-state potential exhibit band gaps, and that the parabolic unoccupied band is split into several bands, similar to the situation in our calculated bands shown in Fig. 7. If the inelastic electron-electron interaction in the final state is taken into account by employing a complex nonlocal self-energy contribution, the gaps in the final bands are closed, flat bands disappear, and the final bands now have a dispersion practically identical to a free-electron parabola (Fig. 9 of Ref. 32). Further, it was shown that this final band couples best to the plane wave in the vacuum region, which corresponds to an electron at the detector. Intuitively, one would expect that an unoccupied band calculated by using the ground-state potential becomes more free-electron-like when the presence of the crystal surface is taken into account, and final-state interactions are included, since the photoexcited-electron state must eventually be similar to a free-electron-like state for the photoelectron to be detected outside the crystal. The calculations of Hora and Scheffler thus lend strong support to the interpretation of spectra with the aid of a free-electron final band commonly used by experimentalists.

ACKNOWLEDGMENTS

Helpful discussions with Franz Himpsel and Eberhardt Dietz are gratefully acknowleged. We are indebted to E. M. Rowe and the staff of the Synchrotron Radiation Center at the University of Wisconsin—Madison for their excellent support. This work was supported by travel grants from the Deutsche Forschungsgemeinschaft through Sonderforschungsbereich 6 and from IBM, Germany.

*Present address: IBM Zürich Research Laboratory, CH-8803 Rüschlikon, Switzerland.

[1]F. J. Himpsel, Appl. Opt. **19**, 3964 (1980), and references therein. For a review, also see E. W. Plummer and W. Eberhardt, [Adv. Chem. Phys. **49**, 533 (1982)] and F. J. Himpsel, [Adv. Phys. **53**, 1 (1983)].

[2]E. Dietz, H. Becker, and U. Gerhardt, Phys. Rev. Lett. **36**, 1397 (1976); E. Dietz and U. Gerhardt, J. Phys. F **8**, 2213 (1978); P. Thiry, O. Chandesris, J. Lecante, C. Guillot, R. Pinchaux, and Y. Petroff, Phys. Rev. Lett. **43**, 82 (1979).

[3]P. Heimann, H. Miosga, and H. Neddermeyer, Solid State Commun. **29**, 463 (1979).

[4]N. E. Christensen, Phys. Status Solidi (B) **54**, 551 (1972); R. Courths, V. Bachelier, and S. Hüfner, Solid State Commun. **38**, 887 (1981).

[5]W. Eberhardt and E. W. Plummer, Phys. Rev. B **21**, 3245 (1980).

[6]See, e.g., F. J. Himpsel and D. E. Eastman, Phys. Rev. B **21**, 3207 (1980); G. Borstel, M. Neumann, and W. Braun, *ibid.* **23**, 3113 (1981); F. J. Himpsel, K. Christmann, P. Heimann, and D. E. Eastman, *ibid.* **23**, 2548 (1981).

[7]J. K. Grepstad and B. J. Slagsvold, Phys. Scr. **25**, 813 (1982).

[8]H. Levinson, F. Greuter, and E. W. Plummer, Phys. Rev. B **27**, 727 (1983).

[9]P. Hofmann, Vacuum **33**, 819 (1983).

[10]F. J. Himpsel, D. E. Eastman, and E. E. Koch, Phys. Rev. B **24**, 1687 (1981).

[11]L. Ley, R. Pollak, S. Kowalczyk, and D. A. Shirley, Phys. Lett. **41A**, 429 (1972).

[12]C. Norris and L. Wallden, J. Phys. F **2**, 180 (1972).

[13]D. E. Eastman, J. Donelon, N. C. Hien, and F. J. Himpsel, Nucl. Instrum. Methods **172**, 327 (1980).

[14]J. R. Anderson and A. V. Gould, Phys. Rev. **139**, A 1459 (1965).

[15]A. J. Arko, D. D. Koelling, and B. Reihl, Phys. Rev. B **27**, 3955 (1983).

[16]G. Jezequel, P. Steiner, F. Solal, A. Barski, R. Pincheaux, and Y. Petroff (unpublished).

[17]G. A. Somorjai and M. A. van Hove, Struct. Bonding (Berlin) **38**, 31 (1979), Fig. 4.4.

[18]E. Dietz and F. J. Himpsel, Solid State Commun. **30**, 235 (1979).

[19]P. J. Feibelman and D. E. Eastman, Phys. Rev. B **10**, 4932 (1974).

[20]J. A. Knapp, F. J. Himpsel, and D. E. Eastman, Phys. Rev. B **19**, 4952 (1979).

[21]P. O. Gartland and B. J. Slagsvold, Phys. Rev. B **12**, 4047 (1975).

[22]F. J. Himpsel and D. E. Eastman, Phys. Rev. Lett. **41**, 507 (1978).

[23]T. L. Loucks, Phys. Rev. Lett. **14**, 1072 (1965).

[24]A. Breeze, Solid State Commun. **14**, 395 (1974).

[25]F. R. McFeeley, L. Ley, S. P. Kowalczyk, and D. A. Shirley, Solid State Commun. **17**, 1415 (1975).

[26]L. Fritsche, M. Rafat, L. Glocker, and J. Noffke, Z. Phys. B **33**, 1 (1979).

[27]See, e.g., J. Noffke, and L. Fritsche, J. Phys. F **12**, 921 (1982).
[28]L. Hedin and B. I. Lundqvist, J. Phys. C **4**, 2064 (1971).
[29]W. J. Looney and J. A. Dreesen, Phys. Rev. B **20**, 3051 (1979).
[30]A. D. Zdetsis, D. A. Papconstantopoulos, and E. N. Economou, J. Phys. F **10**, 1149 (1980).
[31]E. Dietz (private communication).
[32]R. Hora and M. Scheffler, Phys. Rev. B **29**, 692 (1984).

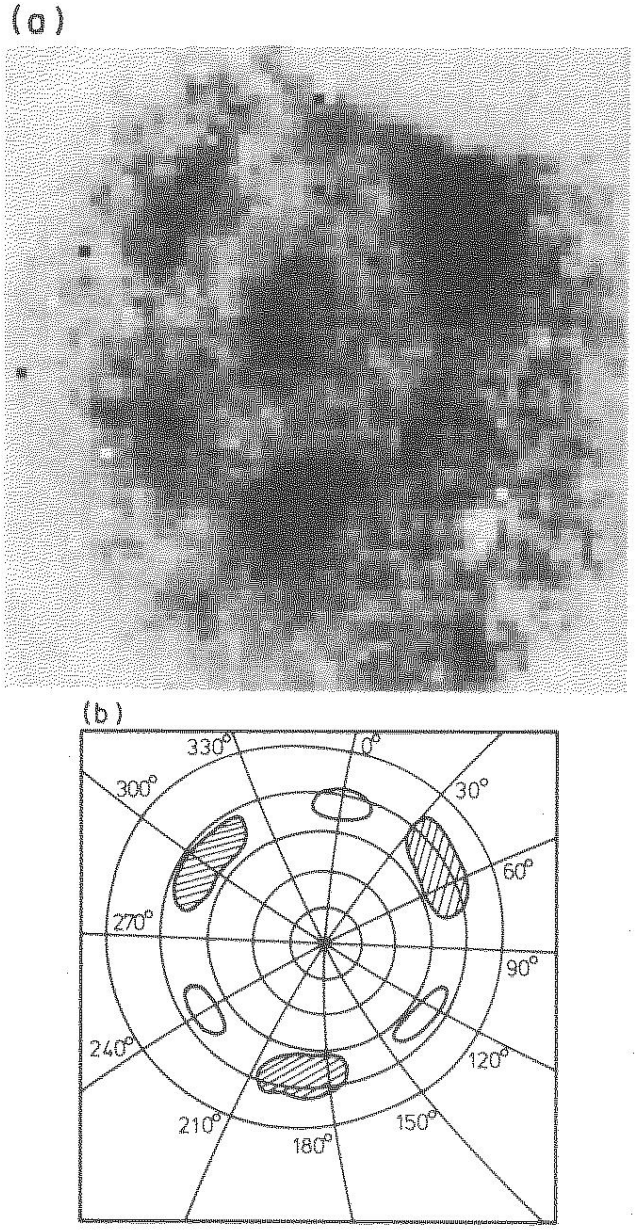

FIG. 5. (a) Photoemission-intensity pattern recorded with the aid of the two-dimensional display electron analyzer at a photon energy of 33 eV and an electron kinetic energy of 26 eV. Dark spots correspond to strong emission. The central spot is the normal-emission direction, while the three dark spots on the outer circle correspond to emission from bands on the $L-K$ line. (b) Sketch of the photoemission-intensity distribution. Polar angles are indicated by distorted circles (for every 5° of emission from normal, which corresponds to the center of the "spider net"). The distortion arises from the geometric arrangement of the channel plates with respect to the axis of the ellipsoidal energy analyzer.